A&A 374, 309–315 (2001)
DOI: 10.1051/0004-6361:20010694


Astronomy & Astrophysics

# Solar differential rotation determined by tracing coronal bright points in SOHO-EIT images

## I. Interactive and automatic methods of data reduction

R. Brajša[1,2,⋆], H. Wöhl[1], B. Vršnak[2], V. Ruždjak[2], F. Clette[3], and J.-F. Hochedez[3]

[1] Kiepenheuer-Institut für Sonnenphysik, Schöneckstr. 6, 79104 Freiburg, Germany
e-mail: hw@kis.uni-freiburg.de
[2] Hvar Observatory, Faculty of Geodesy, University of Zagreb, Kačićeva 26, 10000 Zagreb, Croatia
e-mail: romanb@geodet.geof.hr; bvrsnak@geodet.geof.hr; vruzdjak@geodet.geof.hr
[3] Observatoire Royal de Belgique (ORB), Ave. Circulaire 3, 1180 Bruxelles, Belgium
e-mail: Frederic.Clette@oma.be; hochedez@oma.be

Received 19 February 2001 / Accepted 4 May 2001

**Abstract.** Full-disc solar images obtained with the Extreme Ultraviolet Imaging Telescope (EIT) on board the Solar and Heliospheric Observatory (SOHO) were used to analyse solar differential rotation determined by tracing coronal bright points. Two different procedures were developed and compared: an interactive and an automatic method. The interactive method is based on the visual tracing of coronal bright points in consecutive images using computer programs written in the Interactive Data Language (IDL). The automatic method relies on the IDL procedure "Regions Of Interest (ROI) segmentation" which is used to detect and follow bright points in triplets of consecutive images. The test-results obtained applying both methods by different persons who performed tracing are presented and compared. The advantages and disadvantages of the two methods are discussed.

**Key words.** Sun: corona – Sun: UV radiation – Sun: rotation

## 1. Introduction

Measurements of the solar differential rotation provide an observational constraint on theoretical models of the rotating convection zone and the solar MHD dynamo, which, according to present conceptions, plays a decisive role in generating and maintaining solar magnetic fields and the whole activity of the Sun. The solar surface differential rotation velocity can be determined by two different methods: the Doppler method and the tracer method (Howard 1984; Schröter 1985; Stix 1989; Wöhl 1990, 1997; Snodgrass 1992; Beck 2000). The method based on Doppler shift measurements (e.g., Howard & Harvey 1970; Snodgrass 1984) provides rotational velocities over a broad range of heliographic latitudes, but it is affected by stochastic plasma flows and instrumental effects (e.g., Küveler & Wöhl 1983; Lustig & Wöhl 1989; Wöhl & Schmidt 2000). The other method follows the east-west displacement of distinct features on the solar disc and estimates the corresponding angular rotation velocity. Various features have been used as tracers for solar rotation studies and each has its advantages and disadvantages. For example, the sunspots are well defined structures and live sufficiently long, and so have been most commonly used as tracers (e.g., Balthasar et al. 1986). On the other hand, they have pronounced proper motions during the evolution of active regions. A further disadvantage is that sunspots can be found in only a rather narrow latitude belt, shifting in time towards the equator. Such a problem of a space-time interplay can be avoided using tracers simultaneously present over a broader range of latitudes, e.g., Ca II K mottles (Schröter & Wöhl 1975, 1976), as well as H$\alpha$ filaments and structures in microwaves (e.g., Brajša et al. 1991, 1997). However, one faces the problem of a significant height correction when using H$\alpha$ filaments and microwave structures as tracers (e.g., Aschwanden et al. 1995; Vršnak et al. 1999; Brajša et al. 2000a).

*Send offprint requests to*: R. Brajša,
e-mail: rbrajsa@kis.uni-freiburg.de
⋆ Alexander von Humboldt Research Fellow at the Kiepenheuer-Institut für Sonnenphysik 2000/01.

In this sense coronal bright points are adequate tracers, since they are widely distributed over heliographic latitudes and have small dimensions. Further, the applied height correction will be small, since they are confined to the lower corona of the Sun. Coronal bright points are small-scale bright structures observed in the extreme ultraviolet (EUV) and the X-ray part of the solar spectrum. They have lifetimes from a couple of hours to several days, diameters in the range of 5–20 $\times 10^4$ km and temperatures in the range of 1–3 $\times 10^6$ K (e.g., Benz 1993; Harvey-Angle 1993; Golub & Pasachoff 1997). Although all X-ray bright points can be identified in photospheric magnetograms as small magnetic bipoles, the correlation in the opposite sense is not so definite. It was reported that coronal bright points consist of several small loops (Sheeley & Golub 1979). In addition, high resolution observations performed recently with the TRACE and SOHO spacecrafts revealed their sigmoid fine structure in some cases (Brown et al. 1999).

In this paper, two tracing procedures, an interactive and an automatic one, are proposed and illustrated on a test sample of full-disc solar images from the Extreme Ultraviolet Imaging Telescope (EIT) on board of SOHO. The EIT data set provides a very large set of images obtained with high spatial and temporal resolution. The analysis of such a large data set covering the whole SOHO lifetime requires some type of automatization (e.g., Hochedez et al. 2001). The aim of the present paper is to describe the advantages, disadvantages and limitations of the proposed methods for identifying and tracing coronal bright points.

## 2. The data set

Full-disc solar images from the EIT, taken in the line Fe XV with the 28.4 nm filter, allow detection of small bright structures with high contrast. The EIT instrument was described by Delaboudinière et al. (1995), and the first results were given by Moses et al. (1997). With a telescope focal length of 1.652 m and a square pixel size of 21 × 21 $\mu$m, the plate scale of the EIT images (1024 × 1024 pixels) is 2.629 arcsec per pixel. All necessary information (e.g., the date and time of the exposure, the solar radius and the position of the solar disc centre in the image, etc.) are included in the headers of the image FITS files.

Our test data set consists of 263 full-disc solar images taken during the period from June 4 to December 21, 1998, with a cadence of about 6 hours, with occasional gaps of some 12 hours. There were also some longer interruptions. The images were preprocessed by correcting defects (grid, pre-flight CCD flat-field) and the CCD offset. Many of the images used show small blank rectangular sections (telemetry missing blocks). The images where more than 30% of the solar disc was not covered were excluded (approximately 1% of all images in the test sample). A few entirely unsharp images were also skipped.

In general, EIT images are oriented in such a way that the solar rotation axis is aligned with the $y$-axis of the image. However, after the SOHO loss episode in the summer of 1998 the solar rotation axis was not aligned with the $y$-axis in the images taken from October until mid November 1998. In some images the deviation was up to 20°, and in many cases only a few degrees. Such images constitute about one third of the test data set and were also excluded from the present analysis. These images might be rotated and after the correction of the image orientation included in the reduction, too.

## 3. Interactive method

### 3.1. Description of the method

The interactive method is based on a visual identification of a particular bright point that can be used as a tracer. The programs for the data reduction were written in the Interactive Data Language (IDL). All full-disc solar images from the test data set were visually inspected and the bright points identified in sequences of images. The main criterion for the identification of a bright point was checking its persistence in the consecutive images at approximately the same latitude and shifted in the Central Meridian Distance ($CMD$) according to the elapsed time. This is why the images with the non-aligned rotation axis with the $y$-axis of the image were excluded from the analysis. $CMD$ values of the identified features were then measured in selected consecutive images and were fitted as a function of time ($t$). The correlation coefficient of the function $CMD(t)$ was generally very high, implying that the tracers were correctly identified. The described procedure also enables us to distinguish solar features from the defects caused by cosmic rays, which are not expected to follow the solar rotation.

During the measurements, a 2-dimensional spatial intensity profile of each identified tracer and its intensity variation in time are displayed and the series of heliographic coordinates and times of measurements for each identified tracer are recorded in a file. The spatial resolution of the SOHO-EIT instrument permits an inspection of the fine structure of coronal bright points, and a label indicating the tracer subtype, e.g., point-like structure, small loop or small active region can also be stored. The mean values of the latitude and the $CMD$, as well as the synodic rotation velocity and the meridional velocity are then calculated with their errors and stored. The season dependent transformation from synodic to sidereal rotation velocity was applied (e.g., Roša et al. 1995) taking into account the eccentric orbit of the Earth (as well as SOHO) around the Sun.

### 3.2. Influence of personal judgements on results

The solar differential rotation is most often represented by

$$\omega(b) = A + B\sin^2 b + C\sin^4 b\ , \qquad (1)$$

where $\omega$ is the sidereal angular rotation velocity in degrees per day [$^\circ$ d$^{-1}$], $b$ is the heliographic latitude [$^\circ$], and $A$, $B$, and $C$ are the parameters of the differential rotation curve. In the following, the additional constraint $B = C$ is applied to avoid crosstalk between the parameters $B$ and $C$. This is especially important when the data from middle and higher solar latitudes are considered and when the parameters from different data sets are compared (Scherrer et al. 1980; Brajša et al. 1997, 2000a).

Since the interactive method depends on individual judgements, impressions and estimates, small variations in the application of the method can be expected. In order to estimate these effects on the results, four persons independently performed the tracing of bright points in the same sample of the first 40 images from the test data set (June 4–14, 1998). In the following, the abbreviations MK, JR, HW, and RB are used for the four persons who performed tracing. The general procedure described in Sect. 3.1 was applied, although some differences concerning the duration of tracing and the identification of tracers were adopted. This was described by Brajša et al. (2000b, 2001) who also presented some preliminary results of the interactive method applying the first-order approximation $C = 0$ on the rotation parameters from Eq. (1). All rotation velocities determined by the four persons are presented in Figs. 1–4 in Brajša et al. (2000b), together with the corresponding differential rotation parameters. Differential rotation profiles defined by these parameters are presented by Brajša et al. (2001) together with the mean velocity values. The solar radius used in the coordinate transformation for the June 1998 data corresponds to $704 \times 10^3$ km, which is about $8 \times 10^3$ km larger than the radius of the solar photosphere. Brajša et al. (2000b) show that coronal bright points have no significant height above a solar radius of $704 \times 10^3$ km.

In a preliminary study, Brajša et al. (2000b) introduced a running-average velocity filter over latitudes to reject the statistically unreasonable velocity values due to false identification and inprecise position determination. In the first step of this procedure, rotation velocity parameters defined by Eq. (1) were calculated for all data points for each person separately. Then the half-width of the velocity filter ($\delta$) was specified and the rotation velocities which differ from the mean differential rotation function by $\delta$ were excluded. In the second step, the differential rotation parameters are recalculated for the filtered data. Brajša et al. (2000b) used $\delta = 1.5^\circ$ d$^{-1}$ and since it appeared that a somewhat broader velocity filter should be used, in the present work we apply $\delta = 2.0^\circ$ d$^{-1}$. The results are presented in Table 1 for each of the four persons separately.

The choice for the velocity filter was made by analysing the distribution of the meridional velocity of bright points. This distribution approaches zero at about $1.5^\circ$ d$^{-1}$ and has only an insignificant contribution at velocities larger than $2.0^\circ$ d$^{-1}$. We note that Balthasar et al. (1986) took into account the maximal rotation velocity deviation of $1.0^\circ$ d$^{-1}$, $1.5^\circ$ d$^{-1}$ and $3.0^\circ$ d$^{-1}$ in an analysis of meridional motions of sunspots.

**Table 1.** Differential rotation parameters $A$, $B$, and $C$ from Eq. (1) obtained by four persons with the assumption $B = C$. The interactive method was performed using the images from the interval June 4–14, 1998. Both solar hemispheres were treated together. The sidereal parameters and their standard errors ($M$) expressed in $^\circ$ d$^{-1}$ for all data (a) and for filtered data (f) are presented. The number of used tracers ($n$) is given in the last column.

| Person | $A \pm M_A$ | $-B \pm M_B$ | $-C \pm M_C$ | $n$ |
|---|---|---|---|---|
| MK (a) | 14.30 ± 0.15 | 1.94 ± 0.34 | 1.94 ± 0.34 | 66 |
| MK (f) | 14.35 ± 0.13 | 2.19 ± 0.35 | 2.19 ± 0.35 | 62 |
| JR (a) | 14.29 ± 0.16 | 1.92 ± 0.34 | 1.92 ± 0.34 | 74 |
| JR (f) | 14.29 ± 0.11 | 1.87 ± 0.22 | 1.87 ± 0.22 | 69 |
| HW (a) | 14.38 ± 0.12 | 2.05 ± 0.27 | 2.05 ± 0.27 | 67 |
| HW (f) | 14.44 ± 0.09 | 2.28 ± 0.21 | 2.28 ± 0.21 | 63 |
| RB (a) | 14.29 ± 0.09 | 1.87 ± 0.23 | 1.87 ± 0.23 | 208 |
| RB (f) | 14.28 ± 0.07 | 1.88 ± 0.18 | 1.88 ± 0.18 | 194 |

**Table 2.** The same as in Table 1 for the interval June 4–24, 1998. Parameters were obtained by two persons with the assumptions $C = 0$ and $C = B$.

| Person | $A \pm M_A$ | $-B \pm M_B$ | $-C \pm M_C$ | $n$ |
|---|---|---|---|---|
| HW (a) | 14.46 ± 0.10 | 3.22 ± 0.40 | 0 | 93 |
| HW (f) | 14.44 ± 0.09 | 2.80 ± 0.35 | 0 | 89 |
| HW (a) | 14.40 ± 0.10 | 2.02 ± 0.24 | 2.02 ± 0.24 | 93 |
| HW (f) | 14.45 ± 0.08 | 2.23 ± 0.20 | 2.23 ± 0.20 | 89 |
| RB (a) | 14.53 ± 0.08 | 3.51 ± 0.30 | 0 | 349 |
| RB (f) | 14.43 ± 0.06 | 3.24 ± 0.24 | 0 | 322 |
| RB (a) | 14.42 ± 0.08 | 2.12 ± 0.18 | 2.12 ± 0.18 | 349 |
| RB (f) | 14.34 ± 0.06 | 1.95 ± 0.14 | 1.95 ± 0.14 | 322 |

To study the influence of the length of the analysed time interval, HW and RB applied the interactive method to the whole data sample from June 1998 (59 images taken during June 4–24, 1998). The resulting differential rotation parameters, for the options $C = 0$ and $C = B$, are presented in Table 2 for all data and for the filtered data using $\delta = 2.0^\circ$ d$^{-1}$. The mean rotation velocities for all data points obtained by HW and RB are presented in Fig. 1 together with the differential rotation profiles. The error bars in Fig. 1 are standard errors of the means calculated as $m \times n^{-0.5}$, where $m$ is the standard deviation and $n$ is the the number of data points in the bin.

### *3.3. Application of the improved solar disc coordinates*

The results presented in Tables 1 and 2 and in Fig. 1, as well as those presented in the preliminary reports by Brajša et al. (2000b, 2001) rely on the solar disc coordinates included in the headers of the image FITS files (the solar radius and the position of the solar disc centre in EIT pixels). We will now introduce improved solar disc

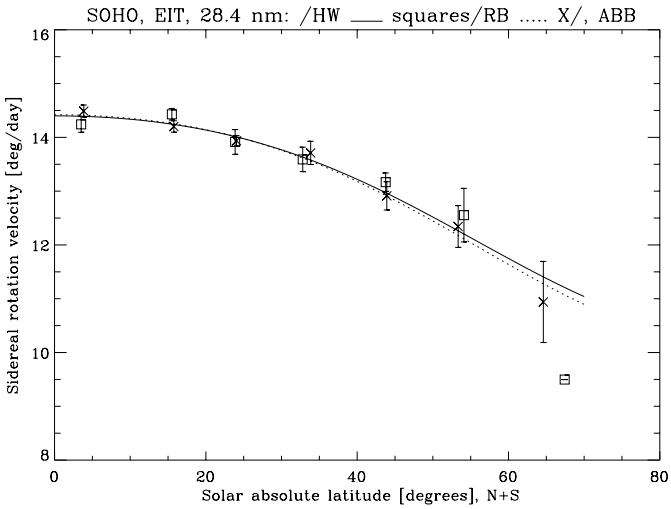


**Fig. 1.** Mean values of sidereal rotation velocities obtained using the interactive method by HW (squares and full line) and RB (crosses and dotted line) in June 4–24, 1998. The measurements were performed in 10° latitude bands and the error bars indicate the standard errors of the means in each bin. Both solar hemispheres were treated together. The lines represent least-squares fits to all data points using $B = C$ (Table 2) for both persons.

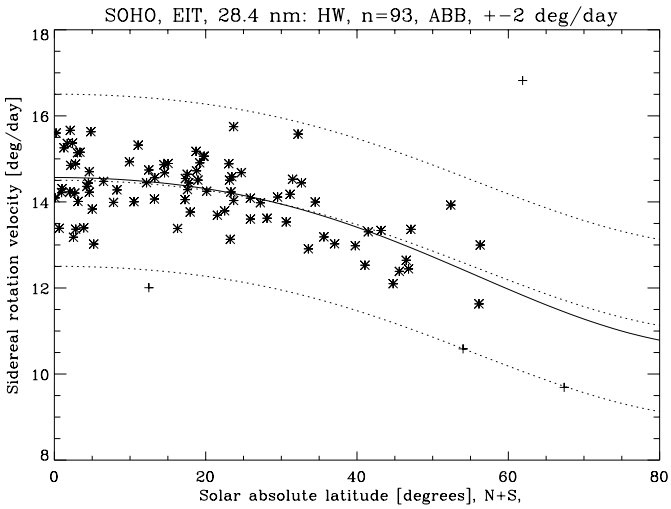


**Fig. 2.** Sidereal rotation velocities obtained using the interactive method and improved solar disc coordinates by HW (data from June 4–24, 1998). Both solar hemispheres were treated together. The data points excluded by the filter are shown by crosses. The fitted differential rotation curve using all data points, as well as the error range $\delta = 2°$ d$^{-1}$, are denoted by the dashed lines. The full line gives the differential rotation curve of the filtered data (stars). The option $B = C$ was applied (Table 3).

coordinates and compare the results obtained by them with those using the original coordinates.

The improved values of the solar radius and the position of the solar disc centre were recalculated using a refined solar limb detection method in the SOHO-EIT images. This was performed by Auchère et al. (1998, their Sect. 3.1) for a long-term analysis of the prolateness of the solar chromosphere. Past experience shows that these improved solar disc coordinates are more accurate and stable in time than the original ones.

We plotted the old solar disc coordinates (from the headers) and the improved ones as a function of time. This confirmed that the random motions of the disc centre coordinates and the solar radius are reduced in the case of the improved coordinates. A continuous trend in the apparent solar radius (as can be seen from SOHO) is also present. This is due to the seasonal variation in the SOHO-Sun distance. Further, meridional motions of coronal bright points for the data from June 4–24, 1998 calculated with the improved solar disc coordinates are smaller, less random and without systematic trends relative to the motions determined using the old coordinates.

HW traced coronal bright points in the images from June 4–24, 1998 using the improved solar disc coordinates. All individual velocity data points are presented in Fig. 2 together with the differential rotation curves determined with all and with just the filtered data. The obtained differential rotation parameters, for the $C = 0$ and $C = B$ options, are presented in Table 3 using $\delta = 2.0°$ d$^{-1}$. Comparing these parameters with the previous ones (Table 2) one finds that the errors became slightly larger when the improved solar disc coordinates were

**Table 3.** The same as in Table 2 for HW and taking into account the improved solar disc coordinates.

| Person | $A \pm M_A$ | $-B \pm M_B$ | $-C \pm M_C$ | $n$ |
|---|---|---|---|---|
| HW (a) | 14.58 ± 0.12 | 2.92 ± 0.46 | 0 | 93 |
| HW (f) | 14.62 ± 0.09 | 3.05 ± 0.40 | 0 | 89 |
| HW (a) | 14.50 ± 0.12 | 1.77 ± 0.28 | 1.77 ± 0.28 | 93 |
| HW (f) | 14.57 ± 0.09 | 1.98 ± 0.26 | 1.98 ± 0.26 | 89 |

applied. Presently we do not have a plausible explanation for this. We note that the same bright points were used, but the position measurements were repeated entirely independently. Mean rotation velocities for all data points obtained by HW using the old and the improved coordinates are presented in Fig. 3 together with the differential rotation profiles. The error bars in Fig. 3 are standard errors as described in the end of Sect. 3.2.

## 4. Automatic method

### 4.1. Identification of tracers

The IDL package offers a special program to handle small sections (subimages, i.e., patterns to be detected) in large images: The method is an application of the procedure "Regions Of Interest (ROI) segmentation". An example given by the authors of IDL is a detection and identification of stars or galaxies within images of galaxy clusters (e.g., Demo ROI in IDL Version 5 and IDL Reference Guide 5.3, Research Systems Inc., Boulder 1999). The adjustable ROI parameters are the sharpness of the

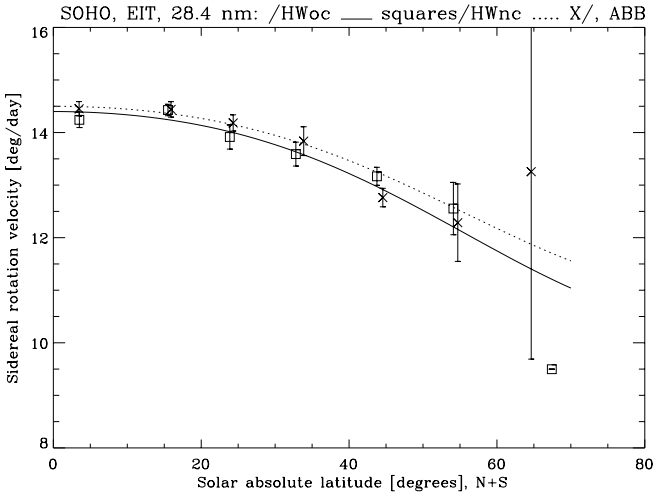


**Fig. 3.** The same as in Fig. 1 for HW and for the two sets of solar disc coordinates: the original ones (squares and the full line) and the improved ones (× and the dotted line).

subimages, their circumference and their brightness. Taking the experience obtained by the interactive method into account, we selected the ROI parameters and called this choice the *first mode* ROI parameters. In this mode, the sharpness – selectable between fuzzy and distinct – was limited from 30 to 255 relative units, the circumference was limited by 20 to 50 pixels and the brightness was limited by 100 to 500 relative intensity units. The centres of the selected small subimages were automatically determined and the cartesian coordinates were transformed to the heliographic ones using the solar disc coordinates given in the headers of the images. The IDL program was developed to identify structures whose latitude does not change more than 1° in consecutive images and for which the synodic rotation velocity lies within the range 9–18° $d^{-1}$. To avoid possible false identifications, the procedure was applied to triplets of consecutive images. The last image of a triplet was taken as the first one of the next triplet. Within the triplets, the time steps from image to image had to be between 5 and 8 hours (in general the step-width was 6 hours). For each identified tracer in a triplet of images, one rotation velocity was calculated by a linear least squares fit $CMD(t)$. Finally, the sidereal rotation velocities were computed from the synodic ones by the transformation mentioned in the end of Sect. 3.1.

Three test-procedures were applied to investigate possible false identification of tracers and their influence on the results of the differential rotation obtained by the automatic method.

(1) The second and third images within triplets were rotated around the solar disc centre with respect to the first images by 45° and 90°, respectively. This method reduced the number of detected structures to less than 2% compared to triplets with correctly aligned images;

(2) 300 artificial objects were randomly distributed over images, which approximately equals the number of structures identified within each image of a triplet by the automatic method. Then, only one bright small structure was identified on average within five triplets, instead of about 35 with the real solar images;

(3) We computed how much a false structure detection, without differential rotation, influences the result of the differential rotation fit. One thousand artificial tracers which obey the differential rotation law $\omega = 14.5 - 3.0 \sin^2 b \pm \delta = 1.0°$ $d^{-1}$ were randomly chosen. Then a fraction of tracers was replaced by the tracers chosen randomly, i.e., without the differential rotation condition. The results were affected significantly only when there was more than 10% of such false identifications in the whole sample.

These tests justified that an application of the automatic method on image triplets provides a reliable automatic identification of small bright tracers in EIT images.

**Table 4.** Differential rotation parameters $A$ and $B$ ($C = 0$) obtained using the automatic method. Tracers were identified applying the *first mode* (f.m.) and the *second mode* (s.m.) as described in text. Sidereal parameters for all data (a) and for filtered data (f) are presented in ° $d^{-1}$ together with their standard errors ($M$). The number of used tracers ($n$) is given in the last column.

| Month 1998 | $A \pm M_A$ | $-B \pm M_B$ | $n$ |
|---|---|---|---|
| June 4–24 (f.m., a) | 14.60 ± 0.14 | 2.75 ± 0.59 | 163 |
| June 4–24 (f.m., f) | 14.57 ± 0.10 | 2.93 ± 0.42 | 143 |
| June 4–24 (s.m., a) | 14.78 ± 0.14 | 2.86 ± 0.59 | 213 |
| June 4–24 (s.m., f) | 14.62 ± 0.10 | 3.09 ± 0.40 | 178 |
| Dec. 1–21 (f.m., a) | 14.79 ± 0.16 | 1.48 ± 0.60 | 132 |
| Dec. 1–21 (f.m., f) | 14.76 ± 0.16 | 1.77 ± 0.43 | 110 |
| Dec. 1–21 (s.m., a) | 14.75 ± 0.14 | 0.99 ± 0.55 | 234 |
| Dec. 1–21 (s.m., f) | 14.70 ± 0.09 | 1.48 ± 0.40 | 184 |

### 4.2. Results

The automatic method was performed by HW on 59 images (21 usable triplets) for the June 1998 data and on 74 images (31 usable triplets) for the December 1998 data. After the *first mode* ROI parameters described in Sect. 4.1 were applied, the procedure was repeated using *second mode* parameters. In the *second mode*, the dynamic range of brightness was increased, allowing relative intensities from 50 to 600 units. The other two ROI parameters, i.e., the sharpness and the circumference, were not changed. The calculated differential rotation parameters with $C = 0$ as well as the number of used tracers are given in Table 4. Filtered structures stem from a region defined by $\delta = 2.0°$ $d^{-1}$ around the mean fitted curve obtained from all structures. The rotation velocities, from which the rotation parameters shown in Table 4 were calculated, were determined using the solar disc coordinates from the headers of the images.

Let us inspect the solar differential rotation parameters and the number of used tracers shown in Table 4. Applying the running velocity filter over latitudes, the number of

**Table 5.** The same as in Table 4 for the *second mode* only and using the improved solar disc coordinates.

| Month 1998 | $A \pm M_A$ | $-B \pm M_B$ | $n$ |
|---|---|---|---|
| June 4–24 (s.m., a) | 14.76 ± 0.12 | 2.42 ± 0.43 | 260 |
| June 4–24 (s.m., f) | 14.66 ± 0.08 | 2.62 ± 0.32 | 225 |
| Dec. 1–21 (s.m., a) | 14.64 ± 0.10 | 2.19 ± 0.29 | 380 |
| Dec. 1–21 (s.m., f) | 14.69 ± 0.07 | 2.62 ± 0.22 | 327 |

tracers was reduced, as some data points fell outside of the imposed limits. The standard errors of the parameters were reduced. Applying the *second mode* of the ROI parameters, the number of identified tracers increased. The standard errors of the rotation parameters were either the same or slightly reduced. In further studies, we will use only the *second mode* ROI parameters in the automatic method, as it provides a larger number of tracers and takes larger brightness variations into account, resembling more the interactive method than the *first mode*.

### 4.3. Application of the improved solar disc coordinates

Using the improved solar disc coordinates described in Sect. 3.3, the number of identified tracers increased significantly using the automatic method, especially in the case of the December 1998 data. In Table 5 the results for the *second mode* ROI parameters applying the improved solar disc coordinates are given. A much larger number of tracers identified in the same data sets justifies the usage of the improved solar disc coordinates. Furthermore, comparing Tables 4 and 5, one finds that the errors of the rotation parameters are smaller in all cases when the improved solar disc coordinates are used.

As an example, the differential rotation velocities for the June 1998 data determined using the *second mode* ROI parameters and improved solar disc coordinates are given in Fig. 4. The complete and the filtered samples are presented. The rotation parameters and the corresponding numbers of tracers are given in the first two rows of Table 5. The mean values of the rotation velocity together with the differential rotation curves (options $C = 0$ and $C = B$) are presented in Fig. 5. The error bars in Fig. 5 are standard errors as described in the end of Sect. 3.2.

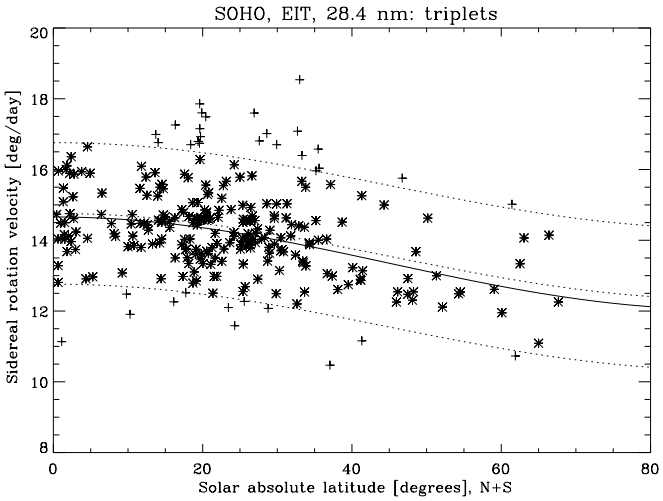


**Fig. 4.** Sidereal rotation velocities obtained using the automatic method (*second mode*; data from June 4–24, 1998) and improved solar disc coordinates. Both solar hemispheres were treated together. The data points excluded by the filter are shown by crosses. The fitted differential rotation curve using all data points, as well as the error range $\delta = 2.0^\circ$ d$^{-1}$, are plotted as dashed lines. The full line gives the differential rotation curve of the filtered data (stars). The option $C = 0$ was applied (Table 5).

## 5. Comparison of the two methods; discussion and conclusion

Let us first discuss the interactive method. The results obtained by the four persons tracing the coronal bright points are not significantly different, in spite of slightly different applications of the interactive method (see Sect. 3.2). This is confirmed by the results of two observers using data over an extended time interval, implying that the results do not depend significantly on the length of the interval. The main advantages of the interactive method are: (1) the high confidence of the tracer identification, (2) the possibility of using different tracing intervals based on the lifetime of the tracer and (3) the possibility of visually identifying the subtype of the bright point tracer (e.g., point-like structure, small loop or small active region) and to follow its evolution. This is important to avoid apparent displacements of the tracer, caused by shape or intensity changes. On the other hand, the main disadvantage of this method is the impossibility of reproducing the results exactly, since it relies on the visual position determination using a computer mouse. Further, the interactive method is very time consuming and hard to perform in comparison with the automatic method. So, the interactive method is not very appropriate for the reduction of larger data sets.

On the other hand, the automatic method is exactly reproducible with the same preset conditions. A comparison of the results from the two methods shows that the interactive method is somewhat more accurate. This can be explained by the longer series of observations (up to 25 images) of identified tracers compared to the automatic method (with only triplets of images). Nevertheless, the differences are not statistically significant even on the $1\sigma$ level. The main advantages of the interactive method mentioned above are at the same time the main disandvantages of the automatic method. On the other hand, the main advantages of the automatic method in comparison to the interactive method are: (1) It allows the selection and reduction of data about five times faster than with the interactive method, and it is far easier. (2) The data reduction is fully reproducible, when applied to the same data sets and selecting the same ROI parameters.

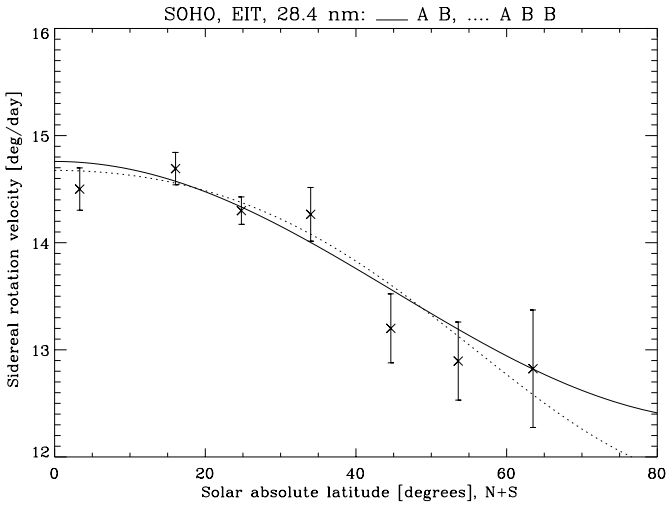


**Fig. 5.** Sidereal rotation velocities obtained applying the automatic method on the data set from June 4–24, 1998 and using the improved coordinates. Mean values were calculated for the 10° latitude bands and the error bars indicate standard errors of the means in each bin. Both solar hemispheres were treated together. The full line represents the fit using $C = 0$ (the parameters are given in the first row in Table 5) and the dotted line represents the fit $A = (14.68 \pm 0.10)^\circ$ d$^{-1}$; $B = C = (-1.45 \pm 0.26)^\circ$ d$^{-1}$ to all data points in both cases.

In the present paper the methods for tracer identification and solar rotation determination in the SOHO-EIT images were described and compared. Various numerical parameters and options were tested and optimal values determined. By this study, the methods are prepared and optimized for more extensive studies of the solar differential rotation. This will include a search for the cycle-related changes of the solar rotation, a comparison of the results obtained with different tracers, and an analysis of large-scale patterns. Finally, the evolution and proper motions of the tracers, as well as their meridional motions and velocity correlations (Reynolds stresses), will be also investigated.

*Acknowledgements.* This work was performed with the support of the Alexander von Humboldt Foundation and is related to the SOHO-EIT Proposal Brajsa_206: "An analysis of the solar rotation velocity by tracing coronal features" (`http://umbra.nascom.nasa.gov/eit/proposals/`) submitted in March 1999 by R. Brajša, B. Vršnak, V. Ruždjak, D. Roša, H. Wöhl, and F. Clette. SOHO is a project of international cooperation between ESA and NASA. We would like to thank the EIT team for developing and operating the instrument. Further, we would like to thank the students M. Kasabašić and J. Rodmann for some data reduction performed with the interactive method and J. Rodmann in addition for several improvements of the IDL programs written to perform these measurements. Finally, F. Clette and J.-F. Hochedez acknowledge the support from the Belgian OSTC and from Prodex.

## References

Aschwanden, M. J., Lim, J., Gary, D. E., & Klimchuk, J. A. 1995, ApJ, 454, 512
Auchère, F., Boulade, S., Koutchmy, S., et al. 1998, A&A, 336, L57
Balthasar, H., Vázquez, M., & Wöhl, H. 1986, A&A, 155, 87
Beck, J. G. 2000, Solar Phys., 191, 47
Benz, A. O. 1993, Plasma Astrophysics (Kluwer, Dordrecht)
Brajša, R., Vršnak, B., Ruždjak, V., et al. 1991, Solar Phys., 133, 195
Brajša, R., Ruždjak, V., Vršnak, B., et al. 1997, Solar Phys., 171, 1
Brajša, R., Ruždjak, V., Vršnak, B., et al. 2000a, Solar Phys., 196, 279
Brajša, R., Wöhl, H., Kasabašić, M., et al. 2000b, Hvar Obs. Bull., 24, 153
Brajša, R., Vršnak, B., Ruždjak, et al. 2001, in ASP Conf. Ser. 200, IAU Symp. 203, Recent Insights into the Physics of the Sun and Heliosphere – Highlights from SOHO and Other Space Missions, ed. P. Brekke, B. Fleck, & J. B. Gurman, in press
Brown, D. S., Parnell, C., Deluca, E., McMullen, R., & Golub, L. 1999, in ASP Conf. Ser., 184, 3rd Advances in Solar Physics Euroconference, Magnetic Fields and Oscillations, ed. B. Schmieder, A. Hofmann, & J. Staude, 81
Delaboudinière, J. P., Artzner, G. E., Brunaud, J., et al. 1995, Solar Phys., 162, 291
Golub, L., & Pasachoff, J. M. 1997, The Solar Corona (Cambridge University Press, Cambridge)
Harvey-Angle, K. L. 1993, Magnetic Bipoles on the Sun, Ph.D. Thesis, University of Utrecht
Hochedez, J.-F., Clette, F., Verwichte, E., Berghmans, D., Cugnon, P. 2001, in ASP Conf. Ser. 200, IAU Symp. 203, Recent Insights into the Physics of the Sun and Heliosphere – Highlights from SOHO and Other Space Missions, ed. P. Brekke, B. Fleck, & J. B. Gurman, in press
Howard, R. 1984, ARA&A, 22, 131
Howard, R., & Harvey, J. W. 1970, Solar Phys., 12, 23
Küveler, G., & Wöhl, H. 1983, A&A, 123, 29
Lustig, G., & Wöhl, H. 1989, A&A, 218, 299
Moses, D., Clette, F., Delaboudinière, J.-P., et al. 1997, Solar Phys., 175, 571
Roša, D., Brajša, R., Vršnak, B., & Wöhl, H. 1995, Solar Phys., 159, 393
Scherrer, P. H., Wilcox, J. M., & Svalgaard, L. 1980, ApJ, 241, 811
Schröter, E. H. 1985, Solar Phys., 100, 141
Schröter, E. H., & Wöhl, H. 1975, Solar Phys., 42, 3
Schröter, E. H., & Wöhl, H. 1976, Solar Phys., 49, 19
Sheeley, N. R., Jr., & Golub, L. 1979, Solar Phys., 63, 119
Snodgrass, H. B. 1984, Solar Phys., 94, 13
Snodgrass, H. B. 1992, in ASP Conf. Ser. 27, 12th Sacramento Peak Summer Workshop, The Solar Cycle, ed. K. L. Harvey, 205
Stix, M. 1989, The Sun (Springer-Verlag, Berlin, Heidelberg)
Vršnak, B., Roša, D., Božić, H., et al. 1999, Solar Phys., 185, 207
Wöhl, H. 1990, in Publ. Debrecen Obs., 7, 6th European Meeting on Solar Physics, The Dynamic Sun, ed. L. Dezsö, 19
Wöhl, H. 1997, Hvar Obs. Bull., 21, 1
Wöhl, H., & Schmidt, W. 2000, A&A, 357, 763